The role of force field parameter uncertainty in the prediction of high pressure viscosities.

Richard A. Messerly

Thermodynamics Research Center, National Institute of Standards and Technology, Boulder, Colorado, 80305

Michelle C. Anderson

Thermodynamics Research Center, National Institute of Standards and Technology, Boulder, Colorado, 80305

S. Mostafa Razavi

Department of Chemical and Biomolecular Engineering, The University of Akron, Akron, Ohio, 44325-3906

J. Richard Elliott

Department of Chemical and Biomolecular Engineering, The University of Akron, Akron, Ohio, 44325-3906

Abstract

Uncertainty estimates increase substantially for high pressures at low reduced temperatures. Nevertheless, a prediction is made for the viscosity of 2,2,4, trimethylhexane at 293K and 1000 MPa, in compliance with the guidelines of the 10th IFPSC.

Keywords:

Uncertainty Quantification, Bayesian Inference, Thermophysical Properties, Shear Viscosity, Molecular Dynamics Simulation, Force Fields, Green-Kubo

1. Introduction

The Industrial Fluid Properties Simulation Challenge (IFPSC) is an open international competition aimed at aligning the molecular simulation community, which is primarily academic, with the goals of industrial research. The present work is a submission to the 10^{th} Industrial Fluid Properties Simulation Challenge (IFPSC10). The 10^{th} challenge is to

Email addresses: richard.messerly@nist.gov (Richard A. Messerly), michelle.anderson@nist.gov (Michelle C. Anderson), sr87@zips.uakron.edu (S. Mostafa Razavi), elliot1@uakron.edu (J. Richard Elliott)

predict the viscosity (η) of 2,2,4-trimethylhexane over a wide range of pressures (P), from 0.1 MPa (atmospheric) to 1000 MPa, at 293 K.

The practical application of IFPSC10 is elastohydrodynamic lubrication (EHL), where knowledge of the pressure-viscosity relationship is paramount. The challenge compound was chosen as an ideal lubricating oil candidate for which no published experimental viscosity data are available above ambient pressure. Experimental measurements have been performed by Scott Bair of Georgia Tech with a sample of greater than 98% purity (Aldrich product number 92470, lot BCBR3588V). The estimated experimental uncertainties for η, T, and P are, respectively, 3%, 0.3 K, and the greater of 1 MPa and 0.4 %.

Classical film thickness formulas rely heavily on the pressure-viscosity coefficient, which is essentially an Arrhenius-like activation parameter. However, faster-than-exponential, a.k.a. super-Arrhenius, dependence on pressure has been observed through experimental viscometery measurements for nearly a century. This super-Arrhenius trend is typically manifest by an inflection point in a plot of $\log_{10}(\eta)$ with respect to pressure. While this behavior is common in experimental measurements, we are not aware of any molecular simulation studies that have addressed this issue. IFPSC10 is an ideal opportunity to demonstrate whether or not molecular simulation can provide evidence supporting or opposing the existence of super-Arrhenius behavior.

To determine an adequate force field for predicting the viscosity-pressure trend, we investigated four different force fields, namely, Transferable Potentials for Phase Equilibria (TraPPE-UA [9, 10, 11]), Transferable Anisotropic Mie (TAMie) [12, 13], Potoff [14, 15], and fourth generation anisotropic-united-atom (AUA4) [16, 17]. Each force field uses a united-atom (UA) Mie λ-6 (generalized Lennard-Jones, LJ) functional form. The comparisons with experimental data were made for saturated liquid viscosity ($\eta_{\text{liq}}^{\text{sat}}$) and compressed liquid viscosity ($\eta_{\text{liq}}^{\text{comp}}$) at 293 K from atmospheric pressure to 1000 MPa. The compounds in question were *n*-alkanes ranging in carbon number from ethane to *n*-docosane and branched alkanes ranging in size from 2-methylpropane to 2,2,4-trimethylpentane. The results for 2,2,4-trimethylpentane at high pressures were especially useful as this com-

pound is a close analogue to the challenge compound and has been well studied experimentally.

While TraPPE and AUA4 (LJ 12-6 based potentials) under predict $\eta_{\mathrm{liq}}^{\mathrm{sat}}$ by greater than 30 % for all compounds studied, TAMie (Mie 14-6) and Potoff (Mie 16-6) predict $\eta_{\mathrm{liq}}^{\mathrm{sat}}$ within 10 % for most compounds. For $\eta_{\mathrm{liq}}^{\mathrm{comp}}$, TAMie is the most reliable at predicting the viscosity-density dependence, while Potoff significantly over estimates $\eta_{\mathrm{liq}}^{\mathrm{comp}}$ with respect to density. However, since Potoff also over estimates pressure at high densities BLANK, the viscosity-pressure trend for Potoff is remarkably accurate even at pressures approaching 1000 MPa. In particular, the Potoff force field predicts the viscosity-pressure trend for 2,2,4-trimethylpentane to within 10 % accuracy. For this reason, we chose to implement the Potoff Mie 16-6 force field for the challenge of predicting η and the pressure-viscosity coefficient of 2,2,4-trimethylhexane. We should note, however, that our previous study did not provide any definitive evidence that the Potoff force field could predict a super-Arrhenius trend for the compounds studied.

One of the entry guidelines for the challenge is "an analysis of the uncertainty in the calculated results." Traditional calculation uncertainties are limited to the random fluctuations of simulation output and/or the uncertainty related to the data post-processing. This class is referred to as "numerical uncertainty" (alternatively referred to as "statistical uncertainty"). Two other classes of uncertainty, namely, "parameter uncertainty" and "functional form uncertainty" (also referred to as "model uncertainty") have been traditionally ignored, although they likely have a greater impact than numerical uncertainty. The latter refers to the uncertainty associated with the choice of force field functional form, while the former refers to the uncertainty in the force field parameters for a given force field functional form.

Quantifying the force field functional form uncertainty is an extremely difficult task, as it often requires considering and performing simulations with numerous functional forms. For this reason, we investigate numerical and parameter uncertainties without addressing functional form uncertainties. Specifically, the chosen functional form is the

same as the Potoff force field, namely, a united-atom, fixed bond length, harmonic angular potential, cosine series torsional potential, and a Mie 16-6 non-bonded potential (see Section 2.3 for details). As previous studies demonstrate the high sensitivity of viscosity on the non-bonded and torsional potentials, we limit our parameter uncertainty investigation to the non-bonded and torsional parameters.

The outline for the present work is the following. Section 2 explains the force field, simulation methodology, and data analysis. Section 3 presents the simulation results, with an emphasis on uncertainty quantification. Section 4 discusses some important observations and limitations. Section 5 recaps the primary conclusions from this work.

2. Methods

2.1. Simulation set-up

Historically, non-equilibrium molecular dynamics (NEMD) has been preferred for highly viscous systems. However, in our recent publication we successfully predicted the viscosity of 2,2,4-trimethylpentane at 293 K and 1000 MPa (the highest pressure required for the challenge) with equilibrium molecular dynamics (EMD). Consistent with our previous study, we use EMD for all pressures in the challenge.

Equilibrium molecular dynamics simulations are performed using GROMACS version 2018 with "mixed" (single and double) precision [24]. GROMACS is compiled using GNU 7.3.0, OpenMPI enabled, and GPU support disabled. The simulations are run using Linux 4.4.0-112-generic x86_64 on an Intel(R) Xeon(R) CPU E5-2699 v4 @ 2.20GHz machine. Example GROMACS input files (.top, .gro. and .mdp) with corresponding shell and python scripts for preparing, running, and analyzing simulations are provided as Supporting Information.

We utilize the same simulation specifications as our previous study BLANK. The general simulation specifications are provided in Table 1. Our previous study demonstrates that, for compounds smaller than *n*-dodecane, the correct system dynamics are obtained using a 2 fs time-step and 1.4 nm non-bonded cut-off distance with analytical tail correc-

tions [25]. Our previous study also shows that finite size effects are negligible for a 400 molecule system.

Table 1: General simulation specifications.

Time-step (fs)	2
Cut-off length (nm)	1.4
Tail-corrections	U and P
Constrained bonds	LINCS [28, 29]
LINCS-order	8
Number of molecules	400

We perform a sequence of six simulation stages: energy minimization, NPT equilibration, NPT production, energy minimization, NVT equilibration, and NVT production. Table 2 lists the integrators, thermostats, barostats, and simulation time used for each NPT and NVT equilibration and production stage. These specifications are also the same as our previous study, with the exception of the NVT production simulation times, which are state point dependent. The specific production times for the NVT production stage are provided in Table 3.

A large number of replicate simulations are required at each state point to improve the precision and to provide more rigorous estimates of uncertainty [6, 30]. We utilize between 30 and 80 independent replicates when simulating the Potoff force field, while we use 200 replicates for the MCMC parameter sets. To ensure independence between replicates, the entire series of simulation stages are repeated for each replicate. The initial energy minimization stage starts with a different pseudo-random configuration while the initial velocities are randomized for each equilibration stage.

2.2. Data analysis

The analysis for the Potoff Mie λ-6 force field simulation results is identical to that prescribed in our previous study (see Reference BLANK). In brief, we implement the

Table 2: Simulation specifications for equilibration (Equil.) and production (Prod.) stages.

	NPT Equil.	NPT Prod.	NVT Equil.	NVT Prod.
Simulation time (ns)	1	1	1	1 to 32
Integrator	Velocity Verlet	Leap frog	Velocity Verlet	Velocity Verlet
Thermostat	Velocity rescale	Nosé-Hoover	Nosé-Hoover	Nosé-Hoover
Thermostat time-constant (ps)	1.0	1.0	1.0	1.0
Barostat	Berendsen	Parrinello-Rahman	N/A	N/A
Barostat time-constant (ps)	1.0	5.0	N/A	N/A
Barostat compressibility (1/bar)	4.5E-5	4.5E-5	N/A	N/A

Table 3: State point specific production times. Pressure is prescribed only in NPT equilibration and production stages.

Pressure (MPa)	NVT Prod. time (ns)
0.1	1
25	1
50	1
100	1
150	1
250	2
400	4
500	8
600	8
700	16
800	16
900	24
1000	32

Green-Kubo "time-decomposition" analysis [6, 30]

$$\eta(t) = \frac{V}{k_{\mathrm{B}} T N_{\mathrm{reps}}} \sum_{n=1}^{N_{\mathrm{reps}}} \int_0^t dt' \left\langle \tau_{\alpha\beta,n}(t') \tau_{\alpha\beta,n}(0) \right\rangle_{t_0,\alpha\beta} \tag{1}$$

where t is time, V is volume, N_{reps} is the number of independent replicate simulations, α and β are $x, y,$ or z Cartesian coordinates, $\tau_{\alpha\beta,n}$ is the α-β off-diagonal stress tensor element for the n^{th} replicate, and $\langle \cdots \rangle_{t_0,\alpha\beta}$ denotes an average over time origins (t_0) and $\tau_{\alpha\beta}$.

$\tau_{\alpha\beta,n}$ is recorded every 6 fs (3 time-steps), Equation 1 averages the independent replicate simulations, twelve different time-origins, and all three unique off-diagonal stress tensor components.

The "true" viscosity, i.e., the infinite-time-limit viscosity, is obtained by evaluating

Equation 1 as $t \to \infty$. As the long-time tail does not converge, we fit the "running integral" to a double-exponential function

$$\eta(t) = A\alpha\tau_1 \left(1 - \exp\left(-t/\tau_1\right)\right) + A(1-\alpha)\tau_2 \left(1 - \exp\left(-t/\tau_2\right)\right) \tag{2}$$

where A, α, τ_1, and τ_2 are fitting parameters and $\eta^\infty = A\alpha\tau_1 + A(1-\alpha)\tau_2$ is the infinite-time-limit viscosity. We fit Equation 2 using a weighted sum-squared-error objective function where the weights are equal to the inverse of the squared standard deviation (σ_η^2). The standard deviation with respect to time of the replicate simulations is fit to the model At^b, where A and b are fitting parameters. To improve the fit of Equation 2, we employ both a long-time and short-time cut-off. Specifically, only data for $t > 3$ ps are included in the fit, while data where $\eta(t) > 0.4 \times \eta^\infty$ are excluded [6, 30].

The uncertainty in η^∞ is obtained by bootstrap re-sampling. Specifically, the fitting process described previously is repeated hundreds of times using randomly selected subsets of replicate simulations. For the Potoff force field, the number of replicates in the subset is equal to the total number of replicates. The methodology is different for the MCMC simulations. In this case, two different rounds of re-sampling are performed. First, only 40 replicates are subsampled from the total of 200 replicates. This is done to randomize the MCMC parameter sets. Second, standard bootstrapping with replacement is performed from these 40 replicates. Both layers of this process are repeated hundreds of times. For both Potoff and MCMC force fields, a 95 % confidence interval is obtained from the distribution of bootstrap estimates for η^∞. An example of the MCMC process is provided in Section SI.II of Supporting Information.

2.3. Force fields

As we demonstrated in our previous study BLANK, the Potoff Mie λ-6 force field provides reliable estimates of the η-P dependence for normal and branched alkanes. In particular, this force field predicts the viscosity within 10 % for 2,2,4-trimethylpentane up to 200 MPa and for propane up to 1000 MPa. By contrast, the TraPPE and TAMie models are c appears to ex being the to

For these reasons, we utilize the Potoff Mie λ-6 force field as the basis for our predictions of η. In addition, we quantify the uncertainties in the non-bonded and torsional parameters. We subsequently propagate these force field parameter uncertainties when predicting η.

The Potoff Mie λ-6 force field utilizes united-atom (UA) sites, where 2,2,4-trimethylhexane is represented with CH_3, CH_2, CH, and C UA sites. Neighboring UA sites are separated by a fixed 0.154 nm bond length. Note that we observed in our previous study that the use of flexible bonds can impact η by several percent.

The angular contribution to energy is computed using a harmonic potential:

$$u^{\text{bend}} = \frac{k_\theta}{2}(\theta - \theta_0)^2 \tag{3}$$

where u^{bend} is the bending energy, θ is the instantaneous bond angle, θ_0 is the equilibrium bond angle (see Table 4), and k_θ is the harmonic force constant with $k_\theta/k_{\text{B}} = 62500\,\text{K/rad}^2$ for all bonding angles, where k_{B} is the Boltzmann constant.

Table 4: Equilibrium bond angles (θ_0) [10, 15]. CH_i and CH_j represent CH_3, CH_2, CH, or C sites.

Bending sites	θ_0 (degrees)
CH_i-CH_2-CH_j	114.0
CH_i-CH-CH_j	112.0
CH_i-C-CH_j	109.5

Dihedral torsional interactions are determined using a modified cosine series:

$$\begin{aligned} u^{\text{tors}} &= c_0 + c_1[1+\cos\phi] + c_2[1-\cos 2\phi] + c_3[1+\cos 3\phi] + A_{\text{s}}\sin^2\left(\frac{3\phi}{2}+180^\circ\right) \\ &= (c_0 - A_{\text{s}}) + c_1[1+\cos\phi] + c_2[1-\cos 2\phi] + \left(c_3 + \frac{A_{\text{s}}}{2}\right)[1+\cos 3\phi] \end{aligned} \tag{4}$$

where u^{tors} is the torsional energy, ϕ is the dihedral angle, c_n are the Fourier constants used in the Potoff force field and listed in Table 5, and $A_{\text{s}}\sin^2\left(\frac{3\phi}{2}+180^\circ\right)$ is an additional term proposed by 7 to shift the torsional barrier heights. Note that ϕ is defined using

a convention similar to IUPAC where $\phi = 180^\circ$ for the *trans* conformation, whereas 7 defines the *trans* conformation as 0° or 360° deg, hence the $+180^\circ$ term. As $\sin^2\left(\frac{3\phi}{2} + 180^\circ\right)$ has a maximum value of 1 at 0°, 120°, 240°, and 360°, u^{tors} is shifted by A_s at these dihedral angles. By contrast, this additional term does not shift u^{tors} for dihedral angles of 0°, 180°, and 300°, which correspond to the equilibrium conformations of *gauche*$^-$, *trans*, and *gauche*$^+$, respectively. Clearly, the non-shifted Potoff torsional potential is obtained only when $A_s = 0$.

Table 5: Fourier constants (c_n/k_B) and shifting parameter (A_s/k_B) in units of K for Potoff force field [10, 15]. CH_i and CH_j represent CH_3, CH_2, CH, or C sites.

Torsion sites	c_0/k_B	c_1/k_B	c_2/k_B	c_3/k_B	A_s/k_B
CH_i-CH_2-CH-CH_j	-251.06	428.73	-111.85	441.27	0.0
CH_i-CH_2-C-CH_j	0.0	0.0	0.0	461.29	0.0

7 set A_s equal to 40% and 15% of the maximum dihedral barrier for the CH_3-CH_2-CH_2-CH_2 and CH_2-CH_2-CH_2-CH_2 torsional potentials, respectively. This corresponds to $A_s/k_B \approx 1000$ K and ≈ 375 K for the CH_3-CH_2-CH_2-CH_2 and CH_2-CH_2-CH_2-CH_2 torsional potentials, respectively. The primary reason why 7 introduced this additional term was to increase the torsional barriers and, thereby, increase the viscosity obtained with the AUA4m force field. This methodology works fairly well for Lennard-Jones 12-6 force fields, which systematically under predict viscosity by greater than 30 %. However, since the Potoff Mie 16-6 potential is already quite reliable for predicting viscosity, we would expect significant over prediction of viscosity if we coupled the Potoff Mie 16-6 potential with $A_s/k_B \gg 0$ K.

The actual reason we include the additional term, however, is to provide a simple method for quantifying the uncertainty in the torsional potential. Specifically, we assume that A_s follows a normal distribution with a mean value of zero and a standard deviation equal to $0.075 \times \max(u^{\text{tors}}_{\text{Potoff}})$ $0.075 \times \max(u^{\text{tors}}_{A_s=0})$. The standard deviation is assigned such

that the 95% confidence interval is equal to 15% the maximum barrier height for the Potoff torsional potential. We use a normal distribution such that the uncertainty in the dihedral barriers is symmetric, i.e., unlike 7 we do not assume that the dihedral barriers must be increased unilaterally. Figure 1 compares the Potoff and MCMC torsional potentials. The insets also depict the normal distribution and the randomly sampled MCMC A_s sets. Note that the challenge compound consists of four $CH_i{-}CH_2{-}CH{-}CH_j$ torsions and three $CH_i{-}CH_2{-}C{-}CH_j$ torsions.

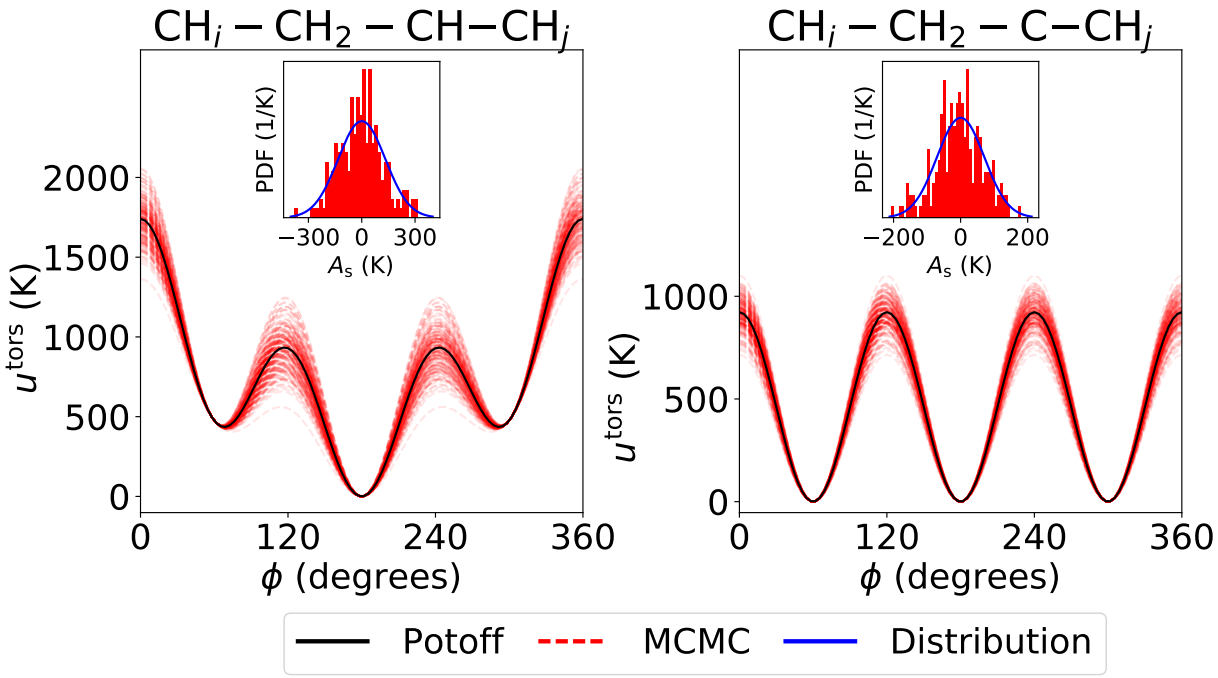

Figure 1: Uncertainty in dihedral potentials. Black line is the Potoff torsional potential. Red lines are the 200 MCMC sampled parameter sets used in this study. Insets show the distribution for A_s. Both u^{tors} and A_s are expressed in units of K, i.e., divided by k_B.

Non-bonded interactions between sites located in two different molecules or separated by more than three bonds within the same molecule are calculated using a Mie λ-6 potential (of which the Lennard-Jones, LJ, 12-6 is a subclass) [31]:

$$u^{vdw}(\epsilon,\sigma,\lambda;r) = \left(\frac{\lambda}{\lambda-6}\right)\left(\frac{\lambda}{6}\right)^{\frac{6}{\lambda-6}}\epsilon\left[\left(\frac{\sigma}{r}\right)^{\lambda}-\left(\frac{\sigma}{r}\right)^{6}\right] \tag{5}$$

where u^{vdw} is the van der Waals interaction, σ is the distance (r) where $u^{vdw} = 0$, $-\epsilon$ is

the energy of the potential at the minimum $\left(\text{i.e., } u^{\text{vdw}} = -\epsilon \text{ and } \frac{\partial u^{\text{vdw}}}{\partial r} = 0 \text{ for } r = r_{\text{min}}\right)$, and λ is the repulsive exponent. The non-bonded Potoff Mie λ-6 force field parameters are provided in Table 6. Note that Potoff reports a "generalized" and "short/long" (S/L) CH and C parameter set. The "short" and "long" parameters are implemented when the number of carbons in the backbone is ≤ 4 and > 4, respectively. The Potoff results presented in this study are obtained with the "long" parameters. (Note that the generalized C parameters are taken from Figure BLANK in Ref. 15 and not from Table BLANK in Ref. 15.)

Table 6: Non-bonded Potoff Mie λ-6 parameters. The "short/long" Potoff CH and C parameters are included in parentheses.

	Potoff (S/L)		
United-atom	ϵ/k_{B} (K)	σ (nm)	λ
CH_3	121.25	0.3783	16
CH_2	61	0.399	16
CH	15 (15/14)	0.46 (0.47/0.47)	16
C	1.05 (1.45/1.2)	0.605 (0.61/0.62)	16

Non-bonded parameters between two different site types (i.e., cross-interactions) are determined using Lorentz-Berthelot combining rules [32] for ϵ and σ and an arithmetic mean for the repulsive exponent λ (as recommended in Reference 14):

$$\epsilon_{ij} = \sqrt{\epsilon_{ii}\epsilon_{jj}} \tag{6}$$

$$\sigma_{ij} = \frac{\sigma_{ii} + \sigma_{jj}}{2} \tag{7}$$

$$\lambda_{ij} = \frac{\lambda_{ii} + \lambda_{jj}}{2} \tag{8}$$

where the ij subscript refers to cross-interactions and the subscripts ii and jj refer to same-site interactions.

The MCMC Mie 16-6 parameters for CH_3 and CH_2 were reported previously. Reference BLANK assumed that the CH_3 parameters were transferable from ethane for longer *n*-alkanes. The CH_2 parameters were obtained from propane, *n*-butane, and *n*-octane. The data included in the analysis were saturated liquid densities and saturated vapor pressures over a reduced temperature range of 0.45 to 0.85, as available in ThermoData Engine (TDE).

The MCMC non-bonded parameters for CH_3 and CH_2 ($\epsilon_{CH_3}, \sigma_{CH_3}, \epsilon_C H_2$, and $\sigma_C H_2$) were reported previously BLANK. These parameters were obtained using a likelihood function based on saturated liquid density and saturated vapor pressure data. By contrast, the MCMC parameters for CH and C ($\epsilon_{CH}, \sigma_{CH}, \epsilon_C$, and σ_C) were obtained from the scoring function reported in 15. Specifically, we assumed a multivariate normal distribution for each ϵ-σ set, where the covariance matrix reproduced the average and covariance matrix were fit to the

such that the short/long

The uncertainty in the CH and C parameter sites were obtained from Reference BLANK. Rather than apply

The following assumptions are made in this uncertainty analysis:

1. CH_3 parameters for ethane are transferable to *n*-alkanes and branched alkanes
2. CH_2 parameters for propane, *n*-butane, and *n*-octane are transferable to branched alkanes
3. CH and C parameters for branched alkanes are transferable to challenge compound
4. Correlation between different UA sites is zero
5. Uncertainty in repulsive exponent (λ) is zero, i.e., we only quantify the uncertainty in ϵ and σ
6. Likelihood function and scoring function only depend on thermodynamic properties at vapor-liquid coexistence conditions

With the assumption of sequential transferability from CH_3

The uncertainty for the non-bonded Mie 16-6 parameter sets in ϵ_{CH_3} non-bonded Mie 16-6 parameters

To simplify the uncertainty analysis, we assume the correlation between Mie parameters of different UA sites is zero. Therefore, we only account for the correlation between ϵ and σ of a given UA site type.

The Potoff "generalized" CH and C parameter set is an attempt at a completely transferable set. However, since the "generalized" parameters performed poorly for some compounds, the S/L parameter set was proposed, where the "short" and "long" parameters are implemented when the number of carbons in the backbone is ≤ 4 and > 4, respectively.

Note that the uncertainties in the CH and C non-bonded parameters are considerably larger than those for CH_3 and CH_2. The CH_3 parameters contribute to the majority of non-bonded interactions (both between different molecules as well as within the same molecule). Therefore, the relatively small uncertainties assigned to the CH_3 parameters are likely the cause for the negligible impact of non-bonded uncertainties.

1. Potoff force field proved to be most reliable in previous study
2. United-atom, Mie 16-6
3. AUA4m considered modifying torsional barriers for CH_2-CH_2 by 15 % and 40 % for internal and terminal torsions, respectively.
4. Include uncertainty in ϵ, σ, and U^{tors}
5. Plots of MCMC samples and maybe the Mie potentials and torsional barriers explicitly

3. Results

Tabulated values for viscosity, density, and pressure at the prescribed state points are provided in Table BLANK. These values are also depicted in Figure BLANK along with the available experimental data point and model fits to simulation data.

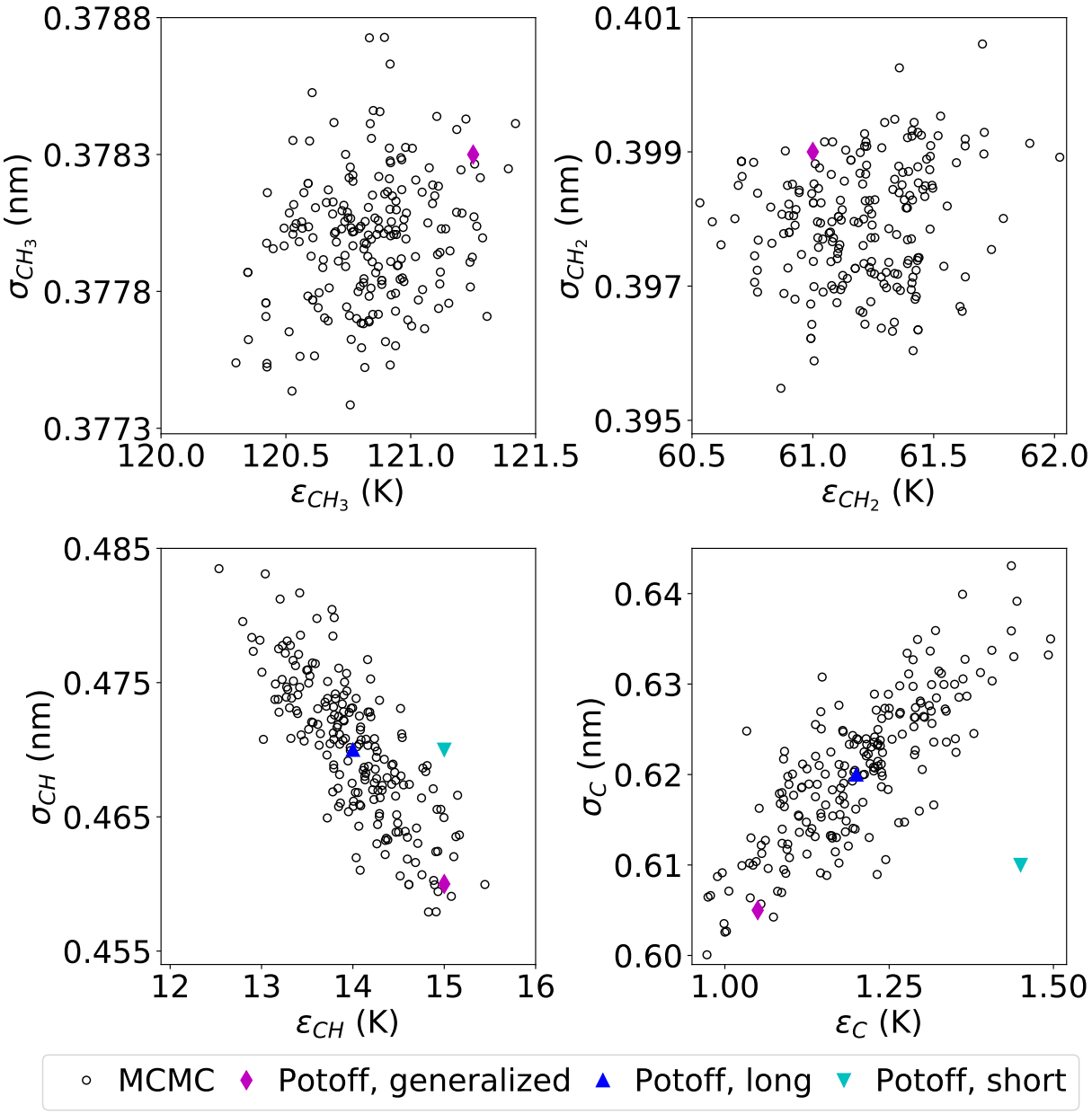

Figure 2: Uncertainty in non-bonded parameters determined with Markov Chain Monte Carlo (MCMC). The Potoff generalized and S/L parameters are also included as a reference. [14, 15]

4. Discussion

Although the deviations from the hybrid McEwen-Paluch model fit to the Potoff-MCMC results are significantly lower than those of the Roelands and Barus models, this

should be anticipated considering the McEwen-Paluch model has five fitting parameters while the Barus and Roelands models only have two.

Although the hybrid McEwen-Paluch model clearly reproduces our simulation results with lower deviations than those of the Roelands and Barus models, this should be anticipated considering the McEwen-Paluch model has five fitting parameters while the Barus and Roelands models only have two.

To quantitatively verify that the Potoff-MCMC force field predicts super-Arrhenius behavior at high pressures, we perform cross-validation between Equations BLANK and BLANK.

The hybrid McEwen-Paluch model is capable of representing an inflection point, i.e., a transition from Arrhenius to super-Arrhenius behavior. By contrast, the Barus and Roelands models are only capable of fitting Arrhenius-like data.

$$\mu = \mu_0 \exp(\alpha P) \tag{9}$$

where μ_0 and α are fitting parameters.

Roelands equation

$$\mu = \mu_p \left(\frac{\mu_0}{\mu_p}\right)^{\left(\frac{P_p - P}{P_p}\right)^Z} \tag{10}$$

where μ_0 and Z are fitting parameters and $\mu_p = 6.31x10^{-}5$ Pa-s and $P_p = -0.196$ GPa.

$$\mu = \mu_0 (1 + \frac{a_0}{q} P)^q \exp\left(\frac{C_{\mathrm{F}} P}{P_\infty - P}\right) \tag{11}$$

where μ_0, a_0, q, C_{F}, and P_∞ are fitting parameters.

Note that the Barus model is obtained from the hybrid McEwen-Paluch model when $a_0 = 0$, $q = 1$, and $P_\infty = P + 1$.

Although the Potoff force field demonstrates super-Arrhenius behavior, we should caution that this could be an anamoly of the force field. Since the Mie 16-6 potential is known to be overly repulsive at short distances, it is possible that this causes the sudden increase in viscosity. This has proven to be the case for the viscosity-density trend, while

we have assumed that the viscosity-pressure trend is reliable due to the simultaneous over prediction of both viscosity and pressure at high densities.

5. Conclusions

Previous work demonstrated that the Potoff force field provides reliable viscosities (typically within 10 %) for well-studied *n*-alkane and branched alkanes both at saturation and elevated pressures. For this reason, the Potoff force field was chosen to predict the viscosity-pressure relationship of 2,2,4-trimethylhexane as part of the 10^{th} Industrial Fluid Properties Simulation Challenge. In addition, we investigate the parameter uncertainty in the simulation results with Bayesian inference. Specifically, the non-bonded and torsional potentials are varied from run to run according to a Markov Chain in force field parameter space.

Furthermore, we assess the existence of so-called super-Arrhenius behavior at high pressures. Cross validation model selection is employed to determine whether a super-Arrhenius empirical equation is required to reproduce our simulation results.

Supporting Information

Section SI.I provides GROMACS input files. Section SI.II outlines the Green-Kubo analysis process.

Acknowledgments

We are grateful for the internal review provided by Andrei F. Kazakov and Alta Y. Fang of the National Institute of Standards and Technology (NIST). This research was performed while Richard A. Messerly held a National Research Council (NRC) Postdoctoral Research Associateship at NIST and while Michelle C. Anderson held a Summer Undergraduate Research Fellowship (SURF) position at NIST.

Commercial equipment, instruments, or materials are identified only in order to adequately specify certain procedures. In no case does such identification imply recom-

mendation or endorsement by NIST, nor does it imply that the products identified are necessarily the best available for the intended purpose.

References

References

[1] E. W. Lemmon, I. H. Bell, M. L. Huber, and M. O. McLinden. NIST Standard Reference Database 23: Reference Fluid Thermodynamic and Transport Properties-REFPROP, Version 10.0, National Institute of Standards and Technology, 2018.

[2] B.E. Poling, J.M. Prausnitz, and J.P. O'Connell. *The Properties of Gases and Liquids, 5th ed.* McGraw-Hill Companies, Inc., 2001. Chapter 9.

[3] Ángel Mulero, Isidro Cachadiña, and José O. Valderrama. Artificial neural network for the correlation and prediction of surface tension of refrigerants. *Fluid Phase Equilibria*, 451:60 – 67, 2017.

[4] Seongmin Lee, Kiho Park, Yunkyung Kwon, Tae-Yun Park, and Dae Ryook Yang. A modified scaled variable reduced coordinate (SVRC)-quantitative structure property relationship (QSPR) model for predicting liquid viscosity of pure organic compounds. *Korean Journal of Chemical Engineering*, 34(10):2715–2724, 2017.

[5] Oliver Lötgering-Lin and Joachim Gross. Group contribution method for viscosities based on entropy scaling using the perturbed-chain polar statistical associating fluid theory. *Industrial & Engineering Chemistry Research*, 54(32):7942–7952, 2015.

[6] Edward J. Maginn, Richard A. Messerly, Daniel J. Carlson, Daniel R. Roe, and J. Richard Elliott. Best practices for computing transport properties 1. Self-diffusivity and viscosity from equilibrium molecular dynamics v1. *Living Journal of Computational Molecular Science*, Pending publication, 2018.

[7] Carlos Nieto-Draghi, Philippe Ungerer, and Bernard Rousseau. Optimization of the anisotropic united atoms intermolecular potential for *n*-alkanes: Improvement of transport properties. *The Journal of Chemical Physics*, 125(4):044517, 2006.

[8] Damien A. Bernard-Brunel and Jeffrey J. Potoff. Effect of torsional potential on the predicted phase behavior of *n*-alkanes. *Fluid Phase Equilibria*, 279(2):100 – 104, 2009.

[9] M. G. Martin and J. I. Siepmann. Transferable potentials for phase equilibria. 1. United-atom description of *n*-alkanes. *The Journal of Physical Chemistry B*, 102(14):2569–2577, 1998.

[10] Marcus G. Martin and J. Ilja Siepmann. Novel configurational-bias monte carlo method for branched molecules. Transferable Potentials for Phase Equilibria. 2. United-Atom Description of Branched Alkanes. *The Journal of Physical Chemistry B*, 103(21):4508–4517, 1999.

[11] Mansi S. Shah, J. Ilja Siepmann, and Michael Tsapatsis. Transferable potentials for phase equilibria. Improved united-atom description of ethane and ethylene. *AIChE Journal*, 63(11):5098–5110, 2017.

[12] Andrea Hemmen and Joachim Gross. Transferable anisotropic united-atom force field based on the Mie potential for phase equilibrium calculations: *n*-alkanes and *n*-olefins. *The Journal of Physical Chemistry B*, 119(35):11695–11707, 2015.

[13] Dominik Weidler and Joachim Gross. Transferable anisotropic united-atom force field based on the Mie potential for phase equilibria: Aldehydes, ketones, and small cyclic alkanes. *Industrial & Engineering Chemistry Research*, 55(46):12123–12132, 2016.

[14] J. J. Potoff and D. A. Bernard-Brunel. Mie potentials for phase equilibria calculations: Applications to alkanes and perfluoroalkanes. *The Journal of Physical Chemistry B*, 113(44):14725–14731, 2009.

[15] Jason R. Mick, Mohammad Soroush Barhaghi, Brock Jackman, Loren Schwiebert, and Jeffrey J. Potoff. Optimized Mie potentials for phase equilibria: Application to branched alkanes. *Journal of Chemical & Engineering Data*, 62(6):1806–1818, 2017.

[16] Philippe Ungerer, Christele Beauvais, Jerome Delhommelle, Anne Boutin, Bernard Rousseau, and Alain H. Fuchs. Optimization of the anisotropic united atoms intermolecular potential for *n*-alkanes. *The Journal of Chemical Physics*, 112(12):5499–5510, 2000.

[17] Carlos Nieto-Draghi, Anthony Bocahut, Benoît Creton, Pascal Have, Aziz Ghoufi, Aurélie Wender, , Anne Boutin, Bernard Rousseau, and Laurent Normand. Optimisation of the dynamical behaviour of the anisotropic united atom model of branched alkanes: application to the molecular simulation of fuel gasoline. *Molecular Simulation*, 34(2):211–230, 2008.

[18] William Allen and Richard L. Rowley. Predicting the viscosity of alkanes using nonequilibrium molecular dynamics: Evaluation of intermolecular potential models. *The Journal of Chemical Physics*, 106(24):10273–10281, 1997.

[19] Rajdeep Singh Payal, S. Balasubramanian, Indranil Rudra, Kunj Tandon, Ingo Mahlke, David Doyle, and Roger Cracknell. Shear viscosity of linear alkanes through molecular simulations: quantitative tests for *n*-decane and *n*-hexadecane. *Molecular Simulation*, 38(14-15):1234–1241, 2012.

[20] Maurizio Mondello and Gary S. Grest. Viscosity calculations of *n*-alkanes by equilibrium molecular dynamics. *The Journal of Chemical Physics*, 106(22):9327–9336, 1997.

[21] Molecular simulation of the thermophysical properties of fluids: From understanding toward quantitative predictions. *Journal of Molecular Liquids*, 134(1):71 – 89, 2007.

[22] Peter A. Gordon. Development of intermolecular potentials for predicting transport properties of hydrocarbons. *The Journal of Chemical Physics*, 125(1):014504, 2006.

[23] Hai Hoang, Stéphanie Delage-Santacreu, and Guillaume Galliero. Simultaneous description of equilibrium, interfacial, and transport properties of fluids using a Mie chain coarse-grained force field. *Industrial & Engineering Chemistry Research*, 56(32):9213–9226, 2017.

[24] M.J. Abraham, D. van der Spoel, E. Lindahl, B.Hess, and the GROMACS development team. *GROMACS User Manual version 2018, www.gromacs.org (2018)*.

[25] GROMACS non-bonded tail corrections assume that the long-range contribution from the $r^{-\lambda}$ term is negligible compared to the r^{-6} term. By comparing the GROMACS output with other (slower) simulation packages, we verified that the small error introduced with this approximation does not significantly affect our results. For this reason, although it is straightforward to include the $r^{-\lambda}$ contribution, we did not attempt to modify the GROMACS default tail correction values.

[26] Vince K. Shen, Daniel W. Siderius, William P. Krekelberg, and Harold W. Hatch. NIST standard reference simulation website, NIST standard reference database number 173. *National Institute of Standards and Technology*, Gaithersburg MD, 20899. https://www.nist.gov/programs-projects/nist-standard-reference-simulation-website. Retrieved July 27, 2018.

[27] Loukas I. Kioupis and Edward J. Maginn. Impact of molecular architecture on the high-pressure rheology of hydrocarbon fluids. *The Journal of Physical Chemistry B*, 104(32):7774–7783, 2000.

[28] Berk Hess, Henk Bekker, Herman J. C. Berendsen, and Johannes G. E. M. Fraaije. LINCS: A linear constraint solver for molecular simulations. *Journal of Computational Chemistry*, 18(12):1463–1472, 1998.

[29] Berk Hess. P-LINCS: A parallel linear constraint solver for molecular simulation. *Journal of Chemical Theory and Computation*, 4(1):116–122, 2008.

[30] Yong Zhang, Akihito Otani, and Edward J. Maginn. Reliable viscosity calculation from equilibrium molecular dynamics simulations: A time decomposition method. *Journal of Chemical Theory and Computation*, 11(8):3537–3546, 2015.

[31] Carmelo Herdes, Tim S. Totton, and Erich A. Müller. Coarse grained force field for the molecular simulation of natural gases and condensates. *Fluid Phase Equilibria*, 406:91 – 100, 2015.

[32] M. P. Allen and D. J. Tildesley. *Computer Simulation of Liquids*. Clarendon Press ; Oxford University Press, Oxford England New York, 1987.